Journal of Alloys and Compounds 690 (2017) 909–915

Contents lists available at ScienceDirect

Journal of Alloys and Compounds

journal homepage: http://www.elsevier.com/locate/jalcom

Spin-phonon coupling in multiferroic Y_2CoMnO_6

Rosivaldo X. Silva [a, b], Manoel C. Castro Júnior [a], Susana Yáñez-Vilar [c, d], Manuel Sánchez Andújar [e], Jorge Mira [c], María Antonia Señarís-Rodríguez [e], Carlos William A. Paschoal [f, *]

[a] Departamento de Física, Universidade Federal do Maranhão, Campus do Bacanga, 65085-580, São Luis, MA, Brazil
[b] Departamento de Física, Universidade Federal do Maranhão, Campus VII, 65400-000, Codó, MA, Brazil
[c] Departamento de Física Aplicada, Universidade de Santiago de Compostela, Campus Sur, 15782, Santiago de Compostela, Spain
[d] Departamento de Física e Astronomía, IFIMUP and IN-Institute of Nanoscience and Nanotechnology, Universidade do Porto, Rúa do Campo Aplegre 687, 4169-007, Porto, Portugal
[e] Grupo QuiMolMat, Departmento de Química Fundamental, Facultad de Ciencias y CICA, Universidade da Coruña, Campus A Coruña, 15071, A Coruña, Spain
[f] Departamento de Física, Universidade Federal do Ceará, Campus do Pici, 65455-900, Fortaleza, CE, Brazil

ARTICLE INFO

Article history:
Received 15 April 2016
Received in revised form
29 June 2016
Accepted 1 July 2016
Available online 2 August 2016

Keywords:
Ceramics
Double perovskite
Magnetostriction
Order-disorder effects
Spin phonon coupling
Raman spectroscopy

ABSTRACT

Spin-phonon coupling in rare-earth based manganites with double perovskite structure plays a crucial role in the magnetoelectric properties of these ferromagnetic materials. Particularly, on Y_2CoMnO_6 (YCMO), it is assumed that spin-phonon coupling is related to the induced ferroelectric polarization. This confers to YCMO a multiferroic characteristic. In this work, we probed the spin-phonon coupling in YCMO by temperature-dependent Raman spectroscopy measurements in ceramic samples obtained by the nitrate decomposition method. Raman scattering revealed some anomalies that could be attributed to a weak spin-phonon coupling, an unconventional behavior for rare-earth based manganites with double perovskite structure, in which the coupling does not fit with the quadratic magnetization.

© 2016 Elsevier B.V. All rights reserved.

1. Introduction

Rare-earth based manganites with double perovskite structure RE_2BMnO_6 (RBMO), in which RE is a rare-earth and B is commonly Ni or Co, has been intensively investigated in last years, mainly due to their multiferroic and magnetoelectric properties [1–4]. In these compounds, as in other perovskites with two different transition metal (TM) cations in the B-sites, there are some factors that can greatly affect the resulting magnetic and electrical properties. Among them, the degree of B–Mn site order, which will decrease as Mn and B ions interchange the occupied sites, the different valencies of the TM cations and the oxygen stoichiometry of the samples.

The ferromagnetic properties of these rare-earth based manganites RE_2BMnO_6 can be well understood on the basis of super-exchange interactions [5]. Nevertheless, their ferroelectric characteristics and the microscopic model to explain the ferroelectric observation, still need more elucidation. For example, in completely disordered La_2NiMnO_6 (LNMO) nanoparticles, Masud et al. [6] observed a relaxor ferroelectric behavior correlated to the ferromagnetism, due to the polarized nano-regions (PNRs) that originated from Ni^{2+} and Mn^{4+} antisite disorder. However, Bahoosh et al. [7] proposed a mechanism in which the ferroelectricity is driven by A-site displacements, as it happens in Bi-based multiferroic systems; while Kumar et al. [3] proposed a model for ferroelectricity, based on density functional theory (DFT) calculations for the Y_2NiMnO_6 (YNMO) perovskite, that is driven by the displacement of all ions. In addition, Lu_2CoMnO_6, which has a strong ferromagnetic-dielectric coupling [8,9], exhibits a magnetic-induced ferroelectric polarization due to magnetic domain boundaries between alternating Co and Mn layers along the c-axis [9].

Recently, Sharma et al. [2] observed a magnetically-induced ferroelectric transition in Y_2CoMnO_6 (YCMO), which undergoes a

* Corresponding author.
E-mail address: paschoal.william@fisica.ufc.br (C.W.A. Paschoal).

http://dx.doi.org/10.1016/j.jallcom.2016.07.010
0925-8388/© 2016 Elsevier B.V. All rights reserved.

ferromagnetic transition at $T_C = 80$ K and this ferromagnetic state generates ferroelectricity. In addition, new interesting properties were observed in this compound, such as disorder-induced exchange bias and multicaloric effects [10,11].

To explain the magnetically-induced ferroelectricity in YCMO Sharma et al. [2] proposed a qualitative model based on the spin-phonon coupling, effect that has been extensively investigated in rare-earth double perovskites [12–18] due to its correlation with magnetodielectric response of RE_2BMO_6 compounds. A powerful tool to detect such coupling, even in systems in which the coupling is weak, is Raman spectroscopy [19–21]. This technique also allows to elucidate the spin-phonon coupling origin, if it is direct or if it is due to magnetostriction [22].

In this work, we have investigated the temperature dependence of the Raman spectra of the ordered YCMO compound in order to understand how the coupling between the lattice and magnetic order happens to obtain information about the mechanism of phase transition, which according to the literature, occurs around $T_C = 80$ K [2].

2. Experimental details

Y_2CoMnO_6 (YCMO) sample was prepared by the nitrate decomposition method. For this purpose, Y_2O_3, previously treated at 1000°C/4 h, was converted into the corresponding nitrate by dissolution in 30% nitric acid. The resulting product was then added to an aqueous solution in which stoichiometric amounts of $Co(NO_3)_2 \cdot 6H_2O$ (Aldrich, 98%) and $Mn(NO_3)_2 \cdot 5H_2O$ (Aldrich, 98%) were also dissolved. The resulting solution was heated to remove the solvent and the organic matter was subsequently decomposed at 400 °C. The obtained precursor powder was ground, pelletized and then treated at 800°C/60 h, 900°C/24 h, 1000°C/24 h and 1100°C/48 h with intermediate regridings. Moreover, in the last two thermal treatments, the sample was slowly cooled to room temperature at 42°C/h.

The crystalline structure of the sample was characterized by X-ray powder diffraction (XRPD) using a Siemens D-5000 diffractometer with Cu (Kα) = 1.5418 Å radiation. XRPD data were collected with a step of 0.015° between 20° and 80° during 12 h and then were inspected using Match software [23] to identify the crystallographic phases present.

In addition, synchrotron X-ray powder diffraction (SXRPD) studies were carried out at 300 K on the BM25A beamline (λ = 0.8261 Å) at the ESRF (Grenoble, France). For this purpose, the samples were loaded in a borosilicate capillary (ϕ = 0.3 mm) and rotated during data collection. The Rietveld analysis were performed with Fullprof program [24], where the atomic positions, lattice and thermal parameters were refined until convergence. The peak shape was described as a pseudo-Voigt function and the background was refined with a 6-coefficients polynomial function. Furthermore, using Bond Valence Sum (BVS) the Mn and Co cations charges were estimated from the obtained bond distances [25,26].

Iodometric titrations were carried out to analyze the oxygen content of the material. For this purpose, the sample was dissolved in acidified KI solutions and the I_2 generated was titrated against a thiosulphate solution. The whole process was carried out under an argon atmosphere.

Magnetic properties were studied in a Quantum Design MPMS SQUID magnetometer. The magnetic susceptibility was measured in the temperature range from 5 K up to 300 K, applying a magnetic field of 1000 Oe. The measurements were performed in cooling conditions without field, ZFC (Zero Field Cooled) and with field, FC (Field Cooled), collecting the data at intervals of 5 K. Hysteresis loops in ZFC conditions were obtained at 5 K varying the field up to ±50 kOe.

Raman spectroscopy measurements were performed in a Horiba spectrometer model iHR550. A 630 nm HeNe laser radiation was taken to the sample through an Olympus microscope model BX30 equipped with a long-working distance objective (20×, 20.5 mm) lens. The scattered light was collected in a Horiba peltier-cooled CCD detector model Synapse. The slits were set to achieve a precision of 1 cm^{-1} in the peak position. Temperature-dependent measurements were performed with the sample inside a He closed-cycle CRYO cryostat, using a temperature controller Lakeshore model 330. The Raman spectra were fitted with lorentzians using the software FitYk (Version 0.9.8).

3. Results and discussions

According to X-ray diffraction measurements this sample is single phase and can be indexed in the monoclinic space group $P2_1/n$. On the other hand, the results of the iodometric titrations indicate that the sample has a very small oxygen deficiency (δ) of 0.02. The room-temperature SXRPD pattern and its refinement are shown in Fig. 1. Following the structure determined for La_2MnCoO_6 [27,28], and a model proposed for Y_2MnCoO_6 [29], the constraint of complete transition-metal cationic ordering was imposed to this refinement (Wyckoff positions 2*c* and 2*b* sites for the Mn and Co cations, respectively). That is, a full Mn–Co B-site order, obtaining a very good agreement. The obtained structure is shown as an inset in Fig. 1. According to this Rietveld refinement, at room temperature YCMO shows lattice parameters $\approx\sqrt{2}\ a_p \times \approx\sqrt{2}\ a_p \times \approx 2a_p$ as indicated in Table 1 (the subscripts "p" refers to the pseudocubic lattice), and Mn–O and Co–O averaged bond distances of 2.11 Å and 1.87 Å, respectively (more details are shown in Table 2). The average superexchange Mn–O–Co angle is around 145°, which is a relatively low angle. This small value is due to the high monoclinic distortion compared to the cubic aristotype structure for double perovskite. When the double perovskites are cubic, they have a Co–O–Mn angle equal to 180°, which gives the maximum superexchange interaction between Co^{2+}(occupied t_{2g} and half-filled e_g orbitals) and Mn^{4+} (occupied t_{2g} and empty e_g orbitals) mediated by oxygens from the Co^{2+}–O–Mn^{4+} bonds [5]. However, due to the small ionic radii of Y, the $(B,Mn)O_6$ octahedra tilts to accommodate

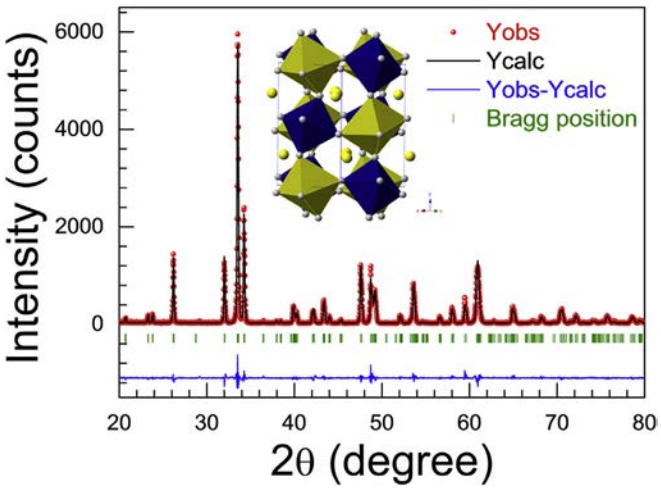

Fig. 1. Synchrotron X-ray powder diffraction data for Y_2CoMnO_6. The red spheres indicate the SXRPD measured data, the black line the SXRPD refined data, the blue line the difference between the measured and the refined data, and the green tickmarcks the positions of the allowed Bragg reflections. The inset shows the unit cell of the here prepared B-site ordered double perovskite Y_2CoMnO_6, which crystallizes in a monoclinic $P2_1/n$ structure. (For interpretation of the references to colour in this figure legend, the reader is referred to the web version of this article.)

Table 1
- Structural parameters of the polycrystalline Y_2CoMnO_6 sample obtained for the Rietveld refinement of the SXRPD pattern. Mn and Co ions are in the 2c and 2b Wyckoff sites, which are special positions with atomic coordinates (½,0,0) and (0,½,0), respectively.

Parameters		Y_2CoMnO_6
Unit cell details		
Space Group		$P2_1/n$
Number of molecules per unit cell, Z		8
Lattice parameters	a (Å)	5.2312 (1)
	b (Å)	5.5859(1)
	c (Å)	7.4694(2)
	β (deg)	89.863(1)
Volume, ($Å^3$)		218.263(9)
Density, (gm/cm^3)		4.12
Independent atomic coordinates		
Y	x	0.5185(3)
	y	0.5725(2)
	z	0.2500(5)
O1	x	0.3942(12)
	y	0.9657(12)
	z	0.2362(20)
O2	x	0.2060(20)
	y	0.1810(20)
	z	−0.0506 (16)
O3	x	0.3290(20)
	y	0.7140(20)
	z	−0.0575(16)
Refinement data		
R_p(%)		9.10
wR_p (%)		12.6
R_{exp}		9.34
χ^2		1.82

the ions originating the monoclinic structure. According to Glazer's notation, this monoclinic structure comes from the cubic one by the octahedral tilt $a^-a^-c^+$ [30]. From the structural data, the octahedral tilts in YCMO are 21.22° and 23.52°. In addition, based on the structural data we have calculated the BVS for YCMO, and the obtained results confirm the presence of Co^{2+} and Mn^{4+} ions in our polycrystalline ceramic, as shown in Table 2.

Fig. 2 shows the temperature dependence of magnetic susceptibility curve obtained for YCMO. As it can be seem from Fig. 2, the reciprocal magnetic susceptibility follows the Curie-Weiss law $\chi^{-1} = (T - \theta)/C$ at high temperatures, whose linear fit shows a

Table 2
– Bond distances of Y_2CoMnO_6 obtained from the Rietvled refinement of the SXRPD pattern. For each bond, the BVS summation for Co and Mn is also indicated.

Bond	Bond length (Å)
Co–O(1)	2.06(2)
Co–O(2)	2.12(1)
Co–O(3)	2.14(1)
BVS	1.91
Mn–O(1)	1.86(1)
Mn–O(2)	1.88(1)
Mn–O(3)	1.88(1)
BVS	4.23
Y–O(1)	2.24(1)
Y–O(1)	2.29(1)
Y–O(2)	2.28(1)
Y–O(2)	2.49(1)
Y–O(3)	2.29(1)
Y–O(3)	2.48(1)
Bond	**Bond angles (°)**
Mn-(O1)–Co	145.1(6)
Mn-(O2)–Co	146.9(5)
Mn-(O3)–Co	144.0(5)

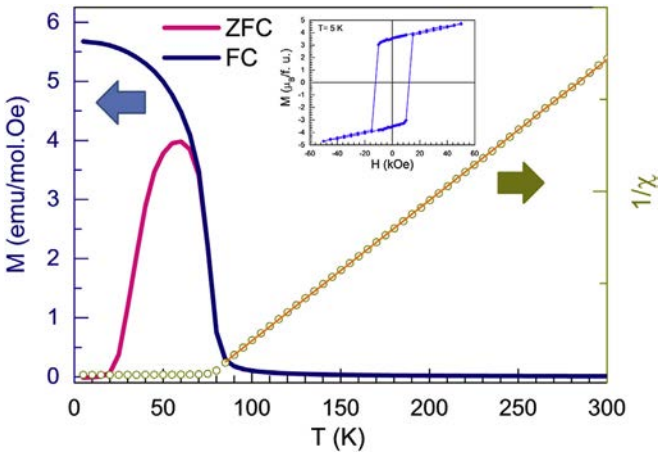

Fig. 2. Left side: Temperature dependence of the magnetic susceptibility for YCMO. The solid blue line corresponds to field cooled (FC) data and the solid pink line to zero field cooled (ZFC) data. **Right side**: Temperature dependence of the reciprocal magnetic susceptibility, represented by dark yellow open circles, and the corresponding linear fit (straight orange line). The inset shows the magnetic hysteresis loop measured at T = 5 K. (For interpretation of the references to colour in this figure legend, the reader is referred to the web version of this article.)

Weiss constant (θ) θ = 80 K, which is a value similar to those obtained by other authors [2,31].

Unfortunately, as the magnetization of this compound did not reach saturation under the maximum field applied, 50 kOe, we could not calculate the magnetic moment per unit formula. The same situation was observed in the case of the closely related Lu_2MnCoO_6 compound, for which a field of 60 T was required to achieve full magnetization [9].

However, the magnetization curve did not exhibit more than one magnetic transition, which is also indicative of a well ordered sample. In addition, considering its oxygen stoichiometry, the results of the structural studies and the BVS calculations are considered, we can assume that the here prepared material is a high quality sample containing the ordered (or almost fully ordered) double perovskite $Y_2Co^{2+}\ Mn^{4+}O_6$ compound.

Fig. 3(a) shows the Raman spectrum recorded for this YCMO sample at T = 10 K. At this temperature, the crystalline structure of YCMO holds the same monoclinic structure belonging to space group $P2_1/n$ observed at room temperature, since no structural phase transitions have been reported for YCMO at low temperatures. Considering the group theory analysis based on site occupation in this structure, 24 Raman-active modes are predicted, whose distribution into the irreducible representation of the 2/m factor group is $12A_g \oplus 12B_g$. As Fig. 3(a) shows, we can observe 10 of these 24 Raman-active modes, but only 5 of these modes are intense enough to be observed in all the temperature range studied. This is a relatively large number of resolved modes at room temperature in based rare-earth manganites with double perovskite structure [32,33]. This can be understood based on the Y^{3+} ionic radius. In general, large ionic rare-earth radii, such as La^{3+} cation, lead to relative minor distortions and small octahedral tilts. Consequently, the emerged modes from the low symmetry show weak intensity at low wavenumbers if we compare them with those of the original cubic $Fm\bar{3}m$ arystotipe lattice [33]. Upon reduction of the ionic radii in the A site, those modes become more intense as observed in the YCMO Raman spectrum, and also in isostructural Y_2NiMnO_6 [16]. Also, more distorted lattices, as it happens when containing RE ions with small ionic radii, tend to split more the degenerate modes due to the distortion.

Previous works were able to define the symmetry of Raman-

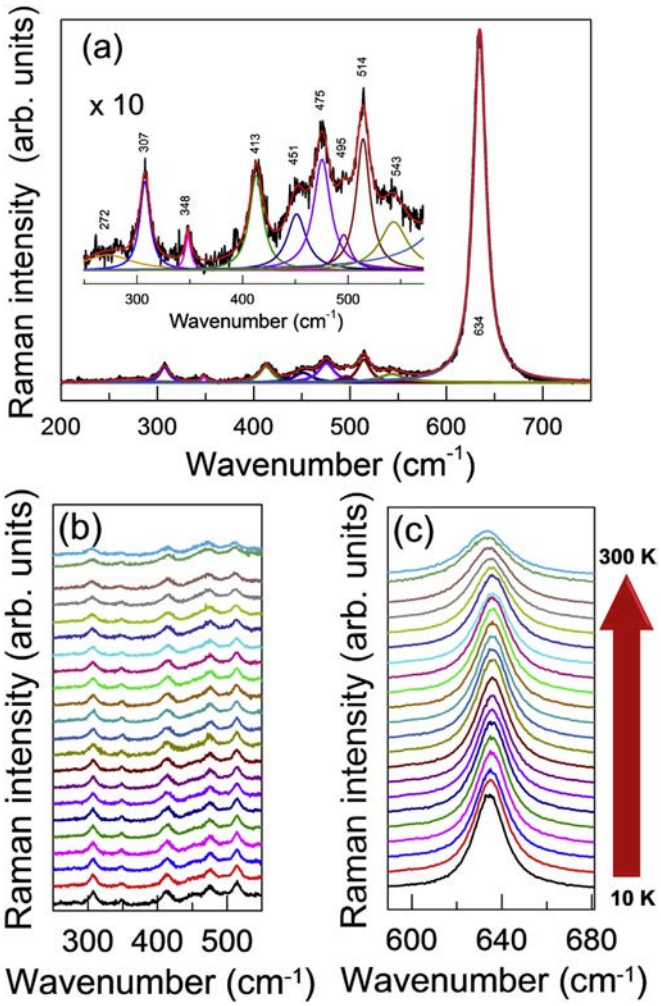

Fig. 3. (a) Raman spectrum of YCMO measured at 10 K. The inset shows the low wavenumber region of the spectrum. Bottom: temperature dependence of the Raman-active phonon spectra in the (b) low wavenumber and (c) high wavenumber region. The temperature measurements were carried out in the temperature interval between 10 and 300 K, in steps of 30 K, except near the magnetic transition, where they were realized every 5 K.

active modes in rare-earth based manganites with double perovskite structure using polarized Raman spectroscopy [33–35]. In YCMO, the spectrum at 10 K is dominated by the commonly observed strong peak, observed at 634 cm^{-1}, which have been assigned to stretching vibrational mode of $(Co/Mn)O_6$, which is like a "breathing" mode, whose symmetry is A_g. At the central part of the spectrum, near the broad band at 543 cm^{-1} and the sharp mode at 514 cm^{-1}, are expected several weak modes of A_g and B_g symmetries associated with octahedra antistretchings or bendings. Also, based on the reported polarized Raman spectra [32–35], the main modes observed at 634, 348, 307 and 272 cm^{-1} can be assigned with A_g symmetry, whereas the modes at 514 and 475 cm^{-1} have B_g symmetry.

Under temperature changes, as the sample was cooled down, a systematic increase in the Raman intensity was observed in both regions of the spectrum. Nevertheless, no remarkable changes were observed in the spectra, which is in agreement with the absence of structural phase transition in this temperature range (see Fig. 3(b) and (c)). The temperature dependence of the main wavenumber positions is shown in Fig. 4. We observe that at least two Raman-active modes show an evident softening near critical temperature $T_C = 80$ K. The position of these modes exhibit a deviation from the expected temperature dependence behavior due to the purely anharmonic contribution, which was modeled by the Balkanski's function [36], as

$$\omega(T) = \omega_o - C\left[1 + \frac{2}{\left(e^{\hbar\omega_o/k_BT} - 1\right)}\right] \quad (1)$$

where C and ω_0 are adjustable parameters, specific for each material and they are indicated as a red line in Fig. 4. This anomalous behavior is commonly associated to the renormalization of the phonons induced by the magnetic ordering due to a coupling between spin and phonons. However, while it is commonly observed only a single spin-phonon coupling in rare-earth based manganites with double perovskite structure when they are B-site ordered [13,16,34,35,37], in YCMO we have observed the spin-phonon coupling at least in two phonons, which is unconventional for double perovskites, where it is observed only in the stretching phonon. This multiple spin-phonon feature was confirmed by the relative Raman intensity of two modes in relation to the stretching one, which is shown in Fig. 5. We can see that the relative intensity of these modes decreases down to a minimum at the magnetic transition and turns to increase again for lower temperatures.

To understand the magnetostriction role in these couplings, we have investigated the dependence of the full-width-at-half-maximum (FWHM) of some selected modes, which is shown in Fig. 6. FWHM is related to the phonon lifetime and is not or slightly affected by magnetostriction features [22,38]. Although we can see a slight plateau between 80 and 40 K in the stretching mode's FWHM, similar to that observed in Tb_2NiMnO_6 (TNMO) [13], this anomaly is very subtle. Also, the other phonons do not exhibit any anomaly. The absence of a remarkable anomaly on FWHM has been associated to spin-phonon coupling driven by magnetostriction effects, as it was observed in other yttrium-based multiferroics [2,39], in which magnetostrinction effects due to the frustration behavior are common [40]. In addition, this result confirms the theoretical predictions by Density Functional Theory (DFT) about the E*-AFM state as the ground state, promoter of magnetostrictive properties of YCMO [41].

Also, according to a mean field approximation and considering nearest neighbor interaction, the spin-phonon coupling contribution to the stretching phonon position in perovskites is given by Ref. [17]:

$$\left|\left(\Delta\omega_{ph}\right)_{stret.}\right| \propto \left(\frac{M(T)}{M_o}\right)^2 \quad (2)$$

In Fig. 7, we compare the position deviation, which is the spin-phonon contribution, of the symmetrical stretching phonon in relation to the square magnetization. We can see clearly that $|\Delta\omega_{ph}|$ does not fit $\left(\frac{M(T)}{M_o}\right)^2$ linearly, as it is shown in Fig. 7. In fact, $|\Delta\omega_{ph}|$ exhibits a squared dependence with the temperature.

This unconventional behavior exhibited by YCMO, compared to other double perovskites, can be associated to a competition between FM and AFM magnetic states due to their frustrated Ising spin chain (E*-type) with ↑↑-↓↓ spin pattern [2,9,40,41]. Also, it can be associated to antisite disorder [30], that might lead to magnetic frustration due the competing magnetic exchange interactions, Co^{2+}–O–Co^{2+} (AFM), Mn^{4+}–O–Mn^{4+} (AFM) and Co^{2+}–O–Mn^{4+} (FM). Order-disorder effects are usual in samples of this compound because of the small difference in charge and ionic radii of the TM occupying the B sites [42]. Nevertheless, the sample studied here shows a large degree of cationic order, even if the presence of a

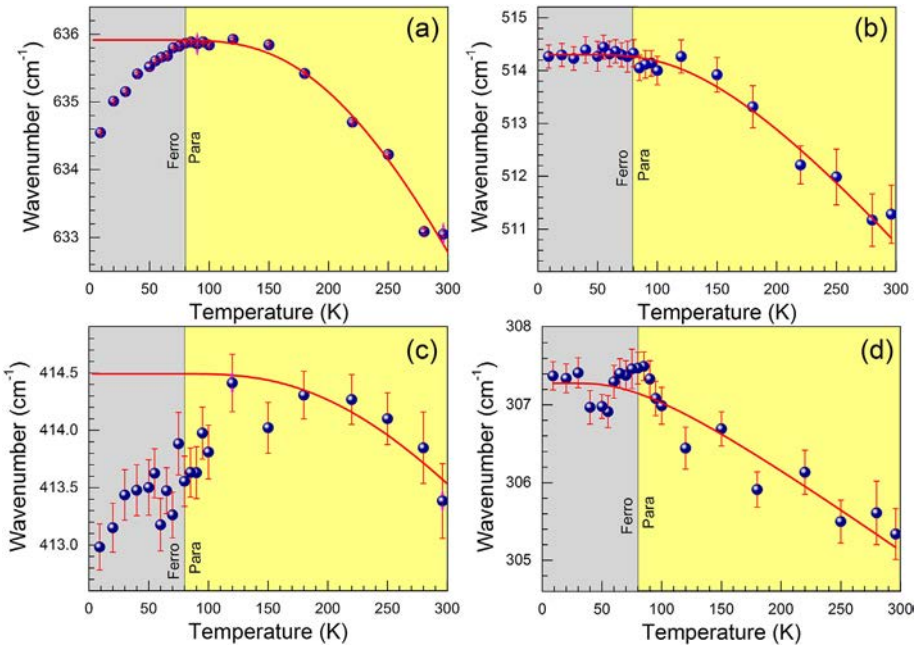

Fig. 4. Temperature dependence of (a) the typical Ag stretching mode, and (b–d) other main modes observed in YCMO. The red line denotes the expected mode position behavior under temperature changes obtained considering only the anharmonic model. (For interpretation of the references to colour in this figure legend, the reader is referred to the web version of this article.)

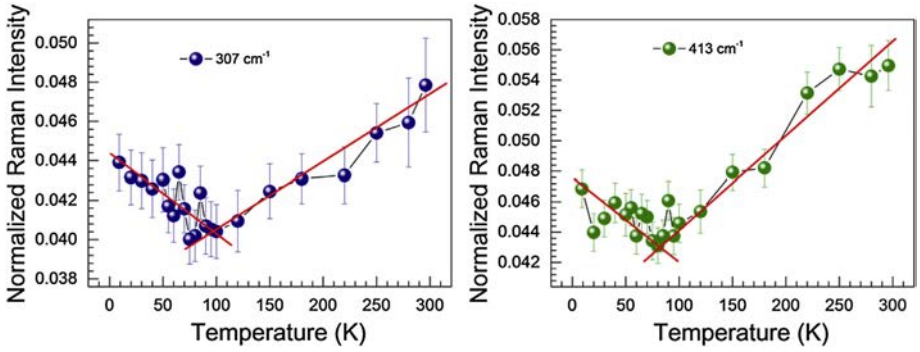

Fig. 5. Temperature dependence of the normalized Raman intensities. The intensity of all present modes were calculated as a function of the intensity of the strongest mode at 634 cm^{-1}.

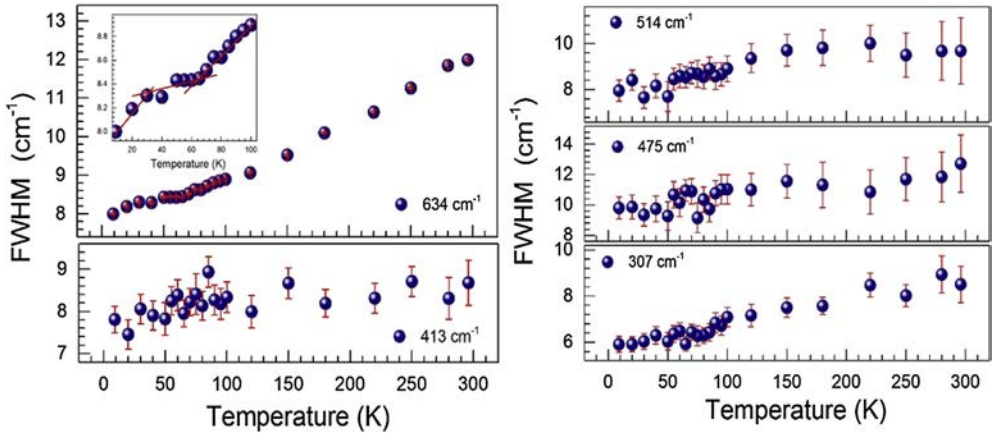

Fig. 6. Temperature dependence of the Raman line widths (FWHM). The inset displays the curve that corresponds to peaks at 634 cm^{-1} that shows a slight slope change between 40 and 80 K.

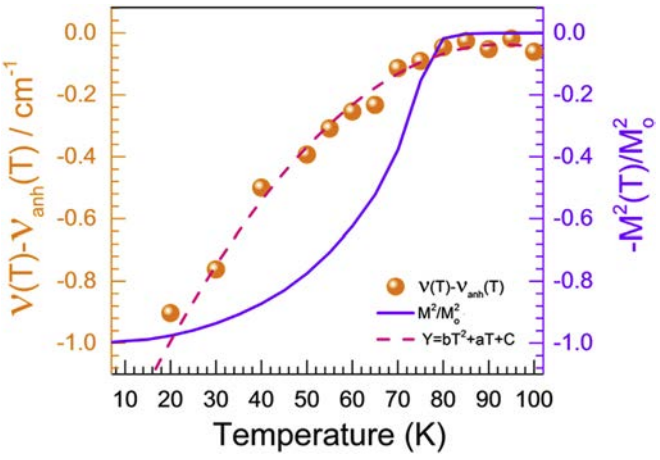

Fig. 7. Temperature dependence of the deviation of the Raman-active stretching mode position observed in relation to the anharmonic phonon contribution.

small amount of antisite disorder (less than 10% [9]) can not be completely discarded and could also contribute to the observed anomaly [31]. Recently, neutron diffraction measurements have confirmed the coexistence of both ferromagnetic and antiferromagnetic interactions in YCMO [2], as it had also the case in the deeply investigated Lu_2MnCoO_6 compound [9]. A similar deviation from the mean field approximation model was observed in the La_2CoMnO_6 spin-phonon analysis [43]. Different value and signals of J_{ij}'s can produce different contributions to the phonon renormalization induced by magnetic ordering, as observed for glassy Gd_2CoMnO_6 [44], which showed a phonon hardening at the magnetic transition, suggesting that the magnitude of the spin-phonon can be turned by the structural order [15]. Also, concerning the Ising chain, a small rare earth ionic radius implies more effective AFM next-nearest-neighbor interactions, which are responsible for the stabilization of the E*-type magnetic structure (for instance a $J_{ij\ Co-Co}$- AFM) [3] turning the spin-phonon coupling more complex, not satisfying the mean field requirements.

4. Conclusions

Raman spectroscopy measurements in the highly B-site ordered Y_2CoMnO_6 double perovskite ceramic obtained by the nitrate decomposition method were able to detect the predicted spin-phonon coupling in this compound at the ferromagnetic transition at 80 K. However, other coupling, different from that usually observed in double perovskites, was also observed. In addition, the spin-phonon coupling observed in the octahedral stretching phonon exhibits a squared dependence with the temperature, which is unconventional for double perovskites. This unconventional behavior exhibited by YCMO compared to other double perovskites can be associated to a competition between FM and AFM magnetic states due to their frustrated Ising spin chain (E*-type) with ↑↑-↓↓ spin pattern. In this case, the small ionic radius of Y^{3+} cation implies more effective AFM next-nearest-neighbor interactions, which are responsible for the stabilization of the E*-type magnetic structure.

Acknowledgements

Brazilian authors acknowledge CNPq (Proc. Number 461621/2014-2), FAPEMA (Proc. Number 02121/12-PRONEM) and CAPES (Proc. Number 552512/2011-7) Brazilian funding agencies. The Spanish authors are grateful for financial support from Ministerio de Economía y Competitividad (Spain) ENE2014-56237-C4-4-R and Xunta de Galicia under the project GRC2014/042. We also thank to the European Synchrotron Radiation Facility for provision of facilities, Germán Castro and Felix Jiménez for the assistance in using beamlineBM25A. S. Y-V acknowledges Xunta de Galicia for a postdoctoral grant (Plan I2C).

References

[1] N.S. Rogado, J. Li, A.W. Sleight, M.A. Subramanian, Magnetocapacitance and magnetoresistance near room temperature in a ferromagnetic semiconductor: La_2NiMnO_6, Adv. Mater 17 (2005) 2225–2227, http://dx.doi.org/10.1002/adma.200500737.
[2] G. Sharma, J. Saha, S.D. Kaushik, V. Siruguri, S. Patnaik, Magnetism driven ferroelectricity above liquid nitrogen temperature in Y_2CoMnO_6, Appl. Phys. Lett. 103 (2013) 012903, http://dx.doi.org/10.1063/1.4812728.
[3] S. Kumar, G. Giovannetti, J. van den Brink, S. Picozzi, Theoretical prediction of multiferroicity in double perovskite Y_2NiMnO_6, Phys. Rev. B 82 (2010) 134429, http://dx.doi.org/10.1103/PhysRevB.82.134429.
[4] J. Krishna Murthy, A. Venimadhav, Magnetodielectric behavior in La_2CoMnO_6 nanoparticles, J. Appl. Phys. 111 (2012) 024102, http://dx.doi.org/10.1063/1.3673862.
[5] J.B. Goodenough, A. Wold, J. Arnott, N. Nenyunk, Relationship Between Crystal Symmetry, Magnetic Properties, Of ionic compounds containing Mn^{3+}, phys. Rev. B 124 (1961) 373–384, http://dx.doi.org/10.1103/PhysRev.124.373.
[6] M.G. Masud, A. Ghosh, J. Sannigrahi, B.K. Chaudhuri, Observation of relaxor ferroelectricity and multiferroic behaviour in nanoparticles of the ferromagnetic semiconductor La_2NiMnO_6, J. Phys. Condens. Matter 24 (2012) 295902, http://dx.doi.org/10.1088/0953-8984/24/29/295902.
[7] S.G. Bahoosh, J.M. Wesselinowa, S. Trimper, The magnetoelectric effect and double-perovskite structure, Phys. Status Solidi 249 (2012) 1602–1606, http://dx.doi.org/10.1002/pssb.201248059.
[8] N. Lee, H.Y. Choi, Y.J. Jo, M.S. Seo, S.Y. Park, Y.J. Choi, Strong ferromagnetic-dielectric coupling in multiferroic Lu_2CoMnO_6 single crystals, Appl. Phys. Lett. 104 (2014) 112907, http://dx.doi.org/10.1063/1.4869479.
[9] S. Yáñez-Vilar, E.D. Mun, V.S. Zapf, B.G. Ueland, J.S. Gardner, J.D. Thompson, et al., Multiferroic behavior in the double-perovskite Lu_2MnCoO_6, Phys. Rev. B 84 (2011) 134427, http://dx.doi.org/10.1103/PhysRevB.84.134427.
[10] J. Krishna Murthy, A. Venimadhav, Multicaloric effect in multiferroic Y_2CoMnO_6, J. Phys. D. Appl. Phys. 47 (2014) 445002, http://dx.doi.org/10.1088/0022-3727/47/44/445002.
[11] H.S. Nair, T. Chatterji, A.M. Strydom, Antisite disorder-induced exchange bias effect in multiferroic Y_2CoMnO_6, Appl. Phys. Lett. 106 (2015) 022407, http://dx.doi.org/10.1063/1.4906204.
[12] M.N. Iliev, H. Guo, A. Gupta, Raman spectroscopy evidence of strong spin-phonon coupling in epitaxial thin films of the double perovskite La_2NiMnO_6, Appl. Phys. Lett. 90 (2007) 151914, http://dx.doi.org/10.1063/1.2721142.
[13] H.S. Nair, D. Swain, H.N.S. Adiga, C. Narayana, S. Elzabeth, Griffiths phase-like behavior and spin-phonon coupling in double perovskite Tb_2NiMnO_6, J. Appl. Phys. 110 (2011) 123919, http://dx.doi.org/10.1063/1.3671674.
[14] K.D. Truong, M.P. Singh, S. Jandl, P. Fournier, Investigation of phonon behavior in Pr_2NiMnO_6 by micro-Raman spectroscopy, J. Phys. Condens. Matter 23 (2011) 052202, http://dx.doi.org/10.1088/0953-8984/23/5/052202.
[15] R.X. Silva, H. Reichlova, X. Marti, D.A.B. Barbosa, M.W. Lufaso, A.P. Ayala, et al., Spin-phonon coupling in $Gd(Co_{1/2}Mn_{1/2})O_3$ perovskite, J. Appl. Phys. 114 (2013) 194102, http://dx.doi.org/10.1063/1.4829902.
[16] R.B. Macedo Filho, A. Pedro Ayala, C. William de Araujo Paschoal, Spin-phonon coupling in Y_2NiMnO_6 double perovskite probed by Raman spectroscopy, Appl. Phys. Lett. 102 (2013) 192902, http://dx.doi.org/10.1063/1.4804988.
[17] E. Granado, A. García, J. Sanjurjo, C. Rettori, I. Torriani, F. Prado, R.D. Sánchez, A. Caneiro, S.B. Oseroff, Magnetic ordering effects in the Raman spectra of $La_{1-x}Mn_{1-x}O_3$, Phys. Rev. B 60 (1999) 11879–11882, http://dx.doi.org/10.1103/PhysRevB.60.11879.
[18] J. Laverdière, S. Jandl, A. Mukhin, V. Ivanov, M. Iliev, Spin-phonon coupling in orthorhombic $RMnO_3$ (R= Pr, Nd, Sm, Eu, Gd, Tb, Dy, Ho, Y): a Raman study, Phys. Rev. B 73 (2006) 214301, http://dx.doi.org/10.1103/PhysRevB.73.214301.
[19] F.M. Silva Júnior, C.W.D.A. Paschoal, Spin-phonon coupling in $BaFe_{12}O_{19}$ M-type hexaferrite, J. Appl. Phys. 116 (2014) 244110, http://dx.doi.org/10.1063/1.4904062.
[20] A. Nonato, B.A. Souza, A.P. Ayala, A.P. Maciel, S. Yañez-Vilar, M. Sanchez-Andujar, M.A. Señaris-Rodríguez, C.W.D.A. Paschoal, Spin-phonon and magnetostriction phenomena in $CaMn_7O_{12}$ helimagnet probed by Raman spectroscopy, Appl. Phys. Lett. 105 (2014) 222902, http://dx.doi.org/10.1063/1.4902234.
[21] Y.P. Santos, B.C. Andrade, R. Machado, M.A. Macêdo, Spin–phonon coupling in multiferroic $Ba_{1.6}Sr_{1.4}Co_2Fe_{24}O_{41}$, J. Magn. Magn. Mater 364 (2014) 95–97, http://dx.doi.org/10.1016/j.jmmm.2014.03.079.
[22] V. Srinu Bhadram, B. Rajeswaran, A. Sundaresan, C. Narayana, Spin-phonon coupling in multiferroic $RCrO_3$ (R-Y, Lu, Gd, Eu, Sm): a Raman study, EPL Europhys. Lett. 101 (2013) 17008, http://dx.doi.org/10.1209/0295-5075/101/17008.

[23] http://www.crystalimpact.com.
[24] J. Rodríguez-Carvajal, Recent advances in magnetic structure determination by neutron powder diffraction, Phys. B Condens. Matter 192 (1993) 55–69, http://dx.doi.org/10.1016/0921-4526(93)90108-I.
[25] I.D. Brown, D. Altermatt, Bond-valence parameters obtained from a systematic analysis of the inorganic crystal structure database, Acta Cryst. B 41 (1985) 244–247, http://dx.doi.org/10.1107/S0108768185002063.
[26] D. Altermatt, I.D. Brown, The automatic searching for chemical bonds in inorganic crystal structures, Acta Cryst. B 41 (1985) 240–244, http://dx.doi.org/10.1107/S0108768185002051.
[27] C.L. Bull, D. Gleeson, K.S. Knight, Determination of B-site ordering and structural transformations in the mixed transition metal perovskites La_2CoMnO_6 and La_2NiMnO_6, J. Phys. Condens. Matter 15 (2003) 4927–4936, http://dx.doi.org/10.1088/0953-8984/15/29/304.
[28] R. Dass, J. Goodenough, Multiple magnetic phases of $La_2CoMnO_{6-\delta}$ (0~δ~0.05), Phys. Rev. B 67 (2003) 014401, http://dx.doi.org/10.1103/PhysRevB.67.014401.
[29] I.O. Troyanchuk, D.D. Khalyavin, J.W. Lynn, R.W. Erwin, Q. Huang, H. Szymczak, et al., Magnetic phase diagrams of the $Ln(Mn_{1-x}Co_x)O_3$ (Ln=Eu, Nd, Y) systems, J. Appl. Phys. 88 (2000) 360, http://dx.doi.org/10.1063/1.373668.
[30] C.J. Howard, B.J. Kennedy, P.M. Woodward, Ordered double perovskites: a group-theoretical analysis, Acta Crystallogr. Sect. B 59 (2003) 463–471, http://dx.doi.org/10.1107/S0108768103010073.
[31] H.S. Nair, R. Pradheesh, Y. Xiao, D. Cherian, S. Elizabeth, T. Hansen, T. Chatterji, Th. Brückel, Magnetization-steps in Y_2CoMnO_6 double perovskite: the role of antisite disorder, J. Appl. Phys. 116 (2014) 123907, http://dx.doi.org/10.1063/1.4896399.
[32] K. Truong, J. Laverdière, M. Singh, S. Jandl, P. Fournier, Impact of Co/Mn cation ordering on phonon anomalies in La_2CoMnO_6 double perovskites: Raman spectroscopy, Phys. Rev. B 76 (2007) 132413, http://dx.doi.org/10.1103/PhysRevB.76.132413.
[33] M. Iliev, M. Abrashev, A. Litvinchuk, V. Hadjiev, H. Guo, A. Gupta, Raman spectroscopy of ordered double perovskite La_2CoMnO_6 thin films, Phys. Rev. B 75 (2007) 104118, http://dx.doi.org/10.1103/PhysRevB.75.104118.
[34] M.N. Iliev, H. Guo, a. Gupta, Raman spectroscopy evidence of strong spin-phonon coupling in epitaxial thin films of the double perovskite La_2NiMnO_6, Appl. Phys. Lett. 90 (2007) 151914, http://dx.doi.org/10.1063/1.2721142.
[35] D. Kumar, S. Kumar, V.G. Sathe, Spin-phonon coupling in ordered double perovskites A_2CoMnO_6 (A = La, Pr, Nd) probed by micro-Raman spectroscopy, Solid State Commun. 194 (2014) 59–64, http://dx.doi.org/10.1016/j.ssc.2014.06.017.
[36] M. Balkanski, R.F. Wallis, E. Haro, Anharmonic effects in light scattering due to optical phonons in silicon, Phys. Rev. B 28 (1983) 1928–1934, http://dx.doi.org/10.1103/PhysRevB.28.1928.
[37] K.D. Truong, M.P. Singh, S. Jandl, P. Fournier, Influence of Ni/Mn cation order on the spin-phonon coupling in multifunctional La_2NiMnO_6 epitaxial films by polarized Raman spectroscopy, Phys. Rev. B 80 (2009) 134424, http://dx.doi.org/10.1103/PhysRevB.80.134424.
[38] H.M. Eiter, P. Jaschke, R. Hackl, A. Bauer, M. Gangl, C. Pfleiderer, A Raman study of the temperature and magnetic field dependence of electronic and lattice properties in MnSi, Phys. Rev. B 90 (2014) 024411, http://dx.doi.org/10.1103/PhysRevB.90.024411.
[39] H. Sakai, J. Fujioka, T. Fukuda, D. Okuyama, D. Hashizume, F. Kagawa, H. Nakao, Y. Murakami, T. Arima, A.Q.R. Baron, Y. Taguchi, Y. Tokura, Displacement-type ferroelectricity with off-center magnetic ions in perovskite $Sr_{1-x}Ba_xMnO_3$, Phys. Rev. Lett. 107 (2011) 137601, http://dx.doi.org/10.1103/PhysRevLett.107.137601.
[40] T. Jia, Z. Zeng, X.G. Li, H.Q. Lin, The magnetic origin of multiferroic Y_2CoMnO_6, J. Appl. Phys. 117 (2015) 17E119, http://dx.doi.org/10.1063/1.4915095.
[41] C.Y. Ma, S. Dong, P.X. Zhou, Z.Z. Du, M.F. Liu, H.M. Liu, Z.B. Yan, J.M. Liu, The ferroelectric polarization of Y_2CoMnO_6 aligns along the b-axis: the first-principles calculations, Phys. Chem. Chem. Phys. 17 (2015) 20961–20970, http://dx.doi.org/10.1039/c5cp02501j.
[42] M.T. Anderson, B.K. Greenwood, G.A. Taylor, K.R. Poeppelmeier, B-cation arrangements in double pervoskites, Prog. Solid State Chem. 22 (1993) 197–233, http://dx.doi.org/10.1016/0079-6786(93)90004-B.
[43] J.K. Murthy, K.D. Chandrasekhar, S. Murugavel, A. Venimadhav, Investigation of the intrinsic magnetodielectric effect in La_2CoMnO_6: role of magnetic disorder, J. Mater. Chem. C 3 (2015) 836–843, http://dx.doi.org/10.1039/C4TC01920B.
[44] X.L. Wang, J. Horvat, H.K. Liu, A.H. Li, S.X. Dou, Spin glass state in Gd_2CoMnO_6 perovskite manganite, Solid State Commun. 118 (2001) 27–30, http://dx.doi.org/10.1016/S0038-1098(01)00033-3.